Journal of Physics G: Nuclear and Particle Physics

PAPER

p-shell hypernuclear energy spectra using the Gogny-interaction shell model

To cite this article: X Y Chen *et al* 2019 *J. Phys. G: Nucl. Part. Phys.* **46** 125106

IOP Publishing Journal of Physics G: Nuclear and Particle Physics
J. Phys. G: Nucl. Part. Phys. **46** (2019) 125106 (15pp) https://doi.org/10.1088/1361-6471/ab4d94

p-shell hypernuclear energy spectra using the Gogny-interaction shell model

X Y Chen, Z Zhou, W G Jiang, B S Hu and F R Xu

School of Physics, and State Key Laboratory of Nuclear Physics and Technology, Peking University, Beijing 100871, People's Republic of China

E-mail: frxu@pku.edu.cn

Received 2 July 2019, revised 27 September 2019
Accepted for publication 14 October 2019
Published 6 November 2019

Abstract

Recent high-resolution experiments at JLab give the energy spectra of the hypernuclei ${}^{7}_{\Lambda}$He, ${}^{9}_{\Lambda}$Li, ${}^{10}_{\Lambda}$Be and ${}^{12}_{\Lambda}$B. However, their spins and parities of the excited states have not been known experimentally. In the present paper, we make a systematical theoretical investigation for the *p*-shell hypernuclei, within the shell model based on the nucleon–nucleon (*NN*) and hyperon–nucleon interactions. The effective *NN* interaction takes the finite-range density-dependent Gogny force, and the hyperon–nucleon interaction takes an empirical ΛN interaction which includes the ΛN–ΣN and ΣN–ΣN coupling effects. The shell model with the Gogny force without parameters being refitted can reasonably describe both spectra and binding energies of the *p*-shell nuclei, which gives a confidence for the further calculations of hypernuclei. We compare our results with experimental data as well as various theoretical calculations, and explain the recent experimental hypernuclear spectra observed at JLab.

Keywords: Λ hypernuclei, energy spectra, Gogny force, ΛN–ΣN coupling, shell model

(Some figures may appear in colour only in the online journal)

1. Introduction

Since the first discovery of the Λ hypernucleus in 1952 [1], the structures of hypernuclei have been studied in order to understand the dynamics of many-body baryon systems and baryon-baryon interactions. Knowledge about the behaviors of hyperons in finite nuclei and hyperon–nucleon interactions needs to be extrapolated to strange hadronic matter [2, 3] and to neutron stars [4, 5].

With effective Λ-nucleon interactions, hypernuclei have been well described using nuclear models such as shell model [6–8], mean-field models [9–14] and beyond-mean-field approaches based on nuclear energy density functionals [15–17]. The pioneering calculations of the shell model by Gal *et al* [6, 18, 19] have successfully explained the γ-ray transitions observed in the *p*-shell Λ hypernuclei [20, 21] and the Λ production cross-sections of the (K^-, π^-) and (π^+, K^+) reactions [22, 23]. The effective Λ*N* interaction used in the calculation is based on the Nijmegen potential, and its validity has been well tested in shell-model [21, 24] and cluster-model calculations [25–27]. More precise calculations need to include the Λ*N*–Σ*N* coupling effect which was first suggested by Akaishi and his collaborators [28, 29] and later tested by *ab initio* calculations using the Nijmegen NSC97 potential [30–32]. Shell-model calculations with the inclusion of the Λ*N*–Σ*N* coupling have been performed by Millener [7, 8] in order to interpret the γ-ray data of the $N \approx Z$ *p*-shell Λ hypernuclei [33]. The effective Λ*N* interaction has also been used to investigate the properties of neutron-rich hypernuclei [34–36], ΛΛ hypernuclei [37] and charge symmetry breaking in Λ hypernuclei [38, 39]. Recently, the advanced hypernuclear no-core–shell model based on chiral effective field theory has been developed and applied to the $A \leqslant 7$ Λ hyperhelium isotopes [40].

The empirical Cohen–Kurath (CK) nucleon–nucleon (*NN*) interaction [41] which was obtained by fitting experimental spectra of nuclei has been widely used in the shell-model calculations of the *p*-shell nuclei. While the interaction has successfully explained the data of $N \approx Z$ Λ hypernuclei, calculations for some neutron-rich hypernuclei, such as ${}^{7}_{\Lambda}$He, deviates from experimental data.

In the calculations of shell-model two-body matrix elements (TBMEs), phenomenological potentials have also been used. Delta-type phenomenological interactions, such as surface delta interaction and Skyrme force, have been adopted in shell-model calculations [42, 43]. In the present work, we use the finite-range density-dependent Gogny force to calculate TBMEs and single-particle energies (SPEs). We use the existing Gogny D1S parameters [44] without refitting. The parameters were determined with mean-field calculations (e.g. Hartree–Fock–Bogoliubov) [45, 46], giving the good descriptions of the bulk properties of nuclei, such as binding energies, charge radii and saturation densities. Previous shell-model calculations based on the Gogny force have successfully explained both binding energies and spectra of the *p*-shell and *sd*-shell nuclei [47], taking the advantage of the density dependence of the Gogny interaction. The present calculations combine the Gogny force and the effective Λ*N* interaction to investigate the *p*-shell hypernuclei. The results are compared with other calculations and the recent experiments performed at JLab.

2. The framework

In the present shell-model calculations of the *p*-shell hypernuclei, ^{4}He is chosen as the frozen core. The Λ or Σ hyperon is assumed to be in the lowest $0s_{1/2}$ orbit, while $(A - 5)$ valence nucleons move in the $0p$ shell. The shell-model TBMEs are calculated using the Gogny force [44] and the Λ*N* interaction [7, 19, 48]. The effective Hamiltonian is given by [7, 35, 48]

$$H = H_0 + V_{NN} + V_{YN}, \tag{1}$$

where $H_0 = \Sigma_a c_a \hat{n}_a$ is the one-body part of the Hamiltonian in the valence space, with c_a and $\hat{n}_a$ being the energy and particle-number operator for the single-particle orbit a, respectively. The Λ hyperon is on the $0s_{1/2}$ orbit, and contributes to H_0 with a constant single-particle energy, thus does not affect the excitation energy spectrum of the hypernucleus. V_{NN} and V_{YN} are the *NN* and hyperon–nucleon interactions, respectively. The hyperon–nucleon interaction

includes the direct ΛN and ΣN interactions, and the ΛN–ΣN and ΣN–ΣN coupling effects [7, 35, 48]. In the presences of the ΛN–ΣN and ΣN–ΣN couplings, the Σ hyperon is included in the model space as the excitation state of the Λ hyperon. The mass difference between Σ and Λ hyperons, i.e. the excitation energy of Λ, is taken as 80 MeV [7, 35, 48].

2.1. The Gogny NN interaction

The *NN* interaction can be written as sum of two-body operators [49]

$$V_{NN} = \sum_{a\leqslant b, c\leqslant d} \sum_{JT} V_{JT}(ab;\, cd)\hat{T}_{JT}(ab;\, cd), \tag{2}$$

with

$$\hat{T}_{JT}(ab;\, cd) = \sum_{J_zT_z} A^{\dagger}_{JJ_zTT_z}(ab)A_{JJ_zTT_z}(cd), \tag{3}$$

where $\hat{T}_{JT}(ab;\, cd)$ is the two-body density operator for the nucleon pair in orbits (a, b) and (c, d) with the coupled angular momentum J and isospin T. $A^{\dagger}_{JJ_zTT_z}$ or $A_{JJ_zTT_z}$ is the creation or annihilation of the nucleon pair. $V_{JT}(ab;\, cd) = \langle a,\, b|V_{NN,\mathrm{Gogny}}|c,\, d\rangle$ is the antisymmetrized TBME for the *NN* interaction. As mentioned already, in the present work, we use the finite-range Gogny force [44]

$$\begin{aligned} V_{NN,\mathrm{Gogny}} = &\sum_{i=1}^{2} \mathrm{e}^{-(\boldsymbol{r}_1-\boldsymbol{r}_2)^2/\mu_i^2}(W_i + B_iP^{\sigma} - H_iP_{\tau} - M_iP^{\sigma}P^{\tau}) \\ &+ t_3\delta(\boldsymbol{r}_1 - \boldsymbol{r}_2)(1 + x_0P^{\sigma})\left[\rho\left(\frac{\boldsymbol{r}_1 + \boldsymbol{r}_2}{2}\right)\right]^{\alpha} \\ &+ \mathrm{i}W_0\delta(\boldsymbol{r}_1 - \boldsymbol{r}_2)(\boldsymbol{\sigma}_1 + \boldsymbol{\sigma}_2)\cdot \boldsymbol{k}' \times \boldsymbol{k}, \end{aligned} \tag{4}$$

to evaluate TBMEs. The Gogny force is density dependent. It has been known that the density dependence which originates from the three-body force plays a crucial role in the calculations of nuclear structure and nuclear matter. In [50], it has been shown that the density dependence is also important for the calculations of nuclear excitation spectra. In our calculations, the density is determined self-consistently by the numerical iteration with the diagonalizing of the shell-model Hamiltonian which is density dependent as well, see [50] for the detailed explanations of the density iteration and *NN* TBME calculations with the Gogny force. The set of most popular parameters D1S [44] is used.

In [47, 50], the feasibility to use the Gogny interaction for the effective shell-model *NN* interaction has been well tested by comparing the TBMEs with those by other effective interactions. Comparisons show good similarity between the TBMEs obtained by the Gogny D1S [44] and by other empirical or realistic interactions in both *p* shell and *sd* shell [47].

2.2. The hyperon–nucleon interaction

The hyperon–nucleon interaction takes the form as [7, 19, 48]

$$V_{YN} = \bar{V} + \Delta\boldsymbol{s}_N\cdot\boldsymbol{s}_Y + S_+\boldsymbol{l}_N\cdot(\boldsymbol{s}_N + \boldsymbol{s}_Y) + S_-\boldsymbol{l}_N\cdot(-\boldsymbol{s}_N + \boldsymbol{s}_Y) + TS_{12}, \tag{5}$$

where Y represents the hyperon (Λ or Σ). $\bar{V}$, Δ, S_+, S_- and T are radial integrals which are parameterized [7, 19, 48]. Using equation (5), the ΛN–ΣN and ΣN–ΣN couplings can be obtained with different parameter values of the radial integrals [7, 19, 35, 48]. $\boldsymbol{s}_N$ and $\boldsymbol{s}_Y$ are spin operators for the nucleon and hyperon, respectively. $\boldsymbol{l}_N$ is the angular momentum operator for the nucleon. The tensor operator S_{12} is defined by

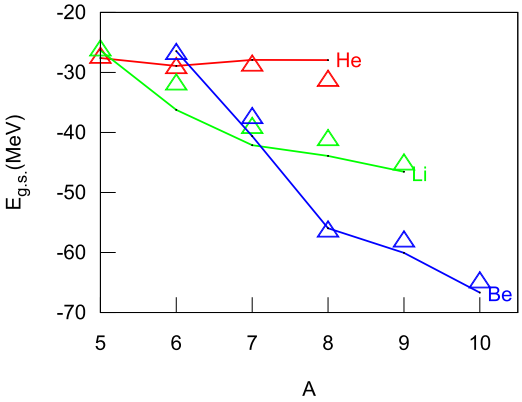

Figure 1. Experimental (triangle) and calculated (line) ground-state energies $E_{\mathrm{g.s.}}$ for helium, lithium and beryllium isotopes. The calculations were done within the shell-model using the Gogny force. The data are taken from [33].

$$S_{12} = 3(\boldsymbol{\sigma}_N \cdot \hat{\boldsymbol{r}})(\boldsymbol{\sigma}_Y \cdot \hat{\boldsymbol{r}}) - \boldsymbol{\sigma}_N \cdot \boldsymbol{\sigma}_Y, \tag{6}$$

with $\boldsymbol{\sigma} = 2\boldsymbol{s}$, and $\hat{\boldsymbol{r}} = (\boldsymbol{r}_N - \boldsymbol{r}_Y)/|\boldsymbol{r}_N - \boldsymbol{r}_Y|$ is the unit vector of the nucleon–hyperon relative coordinate. We adopt the radial integral parameters determined in [7, 8, 34].

3. Calculations of *p*-shell hypernuclei

As a test how well the shell model based on the Gogny force works, we have calculated the ground-state energies of $A \leqslant 9$ helium, lithium and beryllium isotopes with the ^{4}He core, shown in figure 1. We see that the calculations are in good agreement with experimental data. In the calculation, for each nucleus, the length parameter $\hbar\omega$ of the harmonic-oscillator (HO) basis takes the value given by minimizing the energy of the nucleus without the Λ hyperon. In [47], we discussed the $\hbar\omega$ choice. The $\hbar\omega$ value determined thus is close to the empirical value of $\hbar\omega = 45A^{-1/3} - 25A^{-2/3}$ [51]. We have tested that the spectra calculation is not sensitive to the $\hbar\omega$ choice in the range near the minimizing $\hbar\omega$ value. For example, in the ^{6}He case, the energy minimization gives $\hbar\omega = 15.6$ MeV, against the empirical $\hbar\omega = 17.2$ MeV. If we change the $\hbar\omega$ value by 1.0 MeV, i.e. taking $\hbar\omega = 15.6 \pm 1.0$ MeV, the obtained excitation spectrum of $^7_\Lambda$He is almost same as the calculation with $\hbar\omega = 15.6$ MeV. The changes in the excitation energies of the $^7_\Lambda$He $3/2^+$ and $5/2^+$ levels are less than 0.015 MeV. However, nuclear radius calculations would be more sensitive to the choice of $\hbar\omega$ value.

As usual, the Coulomb interaction is not included in the shell-model calculation, to keep the isospin symmetry. It has been known the Coulomb effect on the excitation spectrum of a nucleus is small [52]. However, the Coulomb energy needs to be included in the calculation of nuclear binding energy. In [47], the detailed description of the binding energy calculation has been given, including the calculation of the core energy. It is an advantage of the Gogny-interaction shell model that the core energy can be calculated by the model itself without need of experimental data for the core energy [47]. Another advantage of using the Gogny force is that SPEs can be obtained with the same TBMEs [47] with no need of experimental SPEs. SPEs are important inputs in empirical-interaction shell-model calculations [49].

In the present model, the SPEs are calculated by [47]

$$e_i = t_i + \frac{1}{2(2j+1)} \sum_{i^c} \sum_{JT} (2J+1)(2T+1) \langle i i^c JT | V_{NN,\mathrm{Gogny}} | i i^c JT \rangle, \tag{7}$$

where t_i is the kinetic energy of the ith valence particle. In the HO basis, it is half of the shell energy if we truncate the model space within one major HO shell. For the $0p$ shell, $t_i = \frac{1}{2}\left(2n + l + \frac{3}{2}\right)\hbar\omega = \frac{5}{4}\hbar\omega$ (here $n = 0$ and $l = 1$ for the $0p$ shell). i^c is for an orbit in the core. This means that the single-particle energy is the sum of the kinetic energy and the interaction with all the particles in the core. J and T are the coupled angular momentum and isospin, respectively, which appear already in equation (3). Due to density dependence of the Gogny interaction, the SPEs are nucleus dependent, since different nuclei can have different densities. This means that different SPEs are used for the shell-model calculations of different nuclei. In fact, it is an aspect of self-consistence of the model. For example, with the D1S Gogny force, we obtain the SPEs $e_{0p3/2} = 0.482$ MeV and $e_{0p1/2} = 5.572$ MeV for ^{6}He, while the CK interaction took $e_{0p3/2} = 1.428$ MeV and $e_{0p1/2} = 1.570$ MeV which were obtained as parameters by fitting the experimental spectra of the p-shell nuclei [41]. The experimental SPEs extracted from ^{5}He and ^{4}He data are $e_{0p3/2} = 0.735$ and $e_{0p1/2} = 2.005$ MeV.

We summarize that the present shell model takes ^{4}He as the core, assumes the hyperon staying in the lowest $0s_{1/2}$ orbit and valence nucleons moving in the $0p$ shell. In such calculations, model dimensions are small. The largest dimensions appear in ^{10}B for the nuclei investigated and in $^{11}_{\Lambda}$B for the hypernuclei. The dimension is 84 in ^{10}B, while it is 500 in $^{11}_{\Lambda}$B (with Λ–Σ coupling).

Based on the Gogny NN interaction [44] and the ΛN interaction [7, 19, 35, 48], we have calculated the excitation spectra of the p-shell hypernuclei in which experimental spectra have been available, shown in figures 2 and 3. The spectra of the adjacent nuclei have also been calculated and shown to see how the spectra change with adding a Λ hyperon into the nucleus. We see that the Gogny+ΛN shell-model calculations reproduce well the observed spectra in both hypernuclei and nuclei in this mass region. The results are also consistent with the calculations with the CK NN interaction [41].

The level structure of the $^{12}_{\Lambda}$C hypernucleus was determined at Hyperball2 by recent γ-ray spectroscopy via the ^{12}C(π^+, K$^+\gamma$) reaction [54]. Three experimental excitation levels were determined, corresponding to splitting from the $3/2^-_1$ ground state, $1/2^-_1$ and $3/2^-_2$ excited states in ^{11}C. As shown in figure 4, the Gogny force well reproduces the experimental spectrum. The yet-unobserved $3^-_1 - 2^-_2$ doublet states with a Λ hyperon coupled to the $5/2^-_1$ state of ^{11}C are predicted in the present calculation. For the $3^-_1 - 2^-_2$ doublet, in the earlier publication [55] of the Hyperball2 experiment, the authors reported the $3^-_1 - 2^-_2$ doublet sates which were between doublets $1^-_3 - 2^-_3$ and $0^-_1 - 1^-_2$ [55]. But in their later publication [54], the $3^-_1 - 2^-_2$ doublet states did not appear in the experimental level scheme of the $^{12}_{\Lambda}$C hypernucleus. This would be because no γ rays from the $3^-_1 - 2^-_2$ doublet states had been observed practically.

Recently, the high-resolution spectroscopic experiments for $^7_{\Lambda}$He, $^9_{\Lambda}$Li, $^{10}_{\Lambda}$Be and $^{12}_{\Lambda}$B have been performed at JLab. The mass spectroscopy of the $^7_{\Lambda}$He hypernucleus was performed using the ^{7}Li(e, e'K$^+$)$^7_{\Lambda}$He reaction [56]. As shown in figure 5, two levels were observed where the lower level was assigned as the ground state and the higher level was assigned as a mixture of $3/2^+$ and $5/2^+$ states, supporting the 'gluelike' behavior of the Λ hyperon. In figure 5, we compare our calculations with other theoretical calculations [57, 58]. It is found that the Gogny+ΛN model is consistent with those calculated in [57, 58].

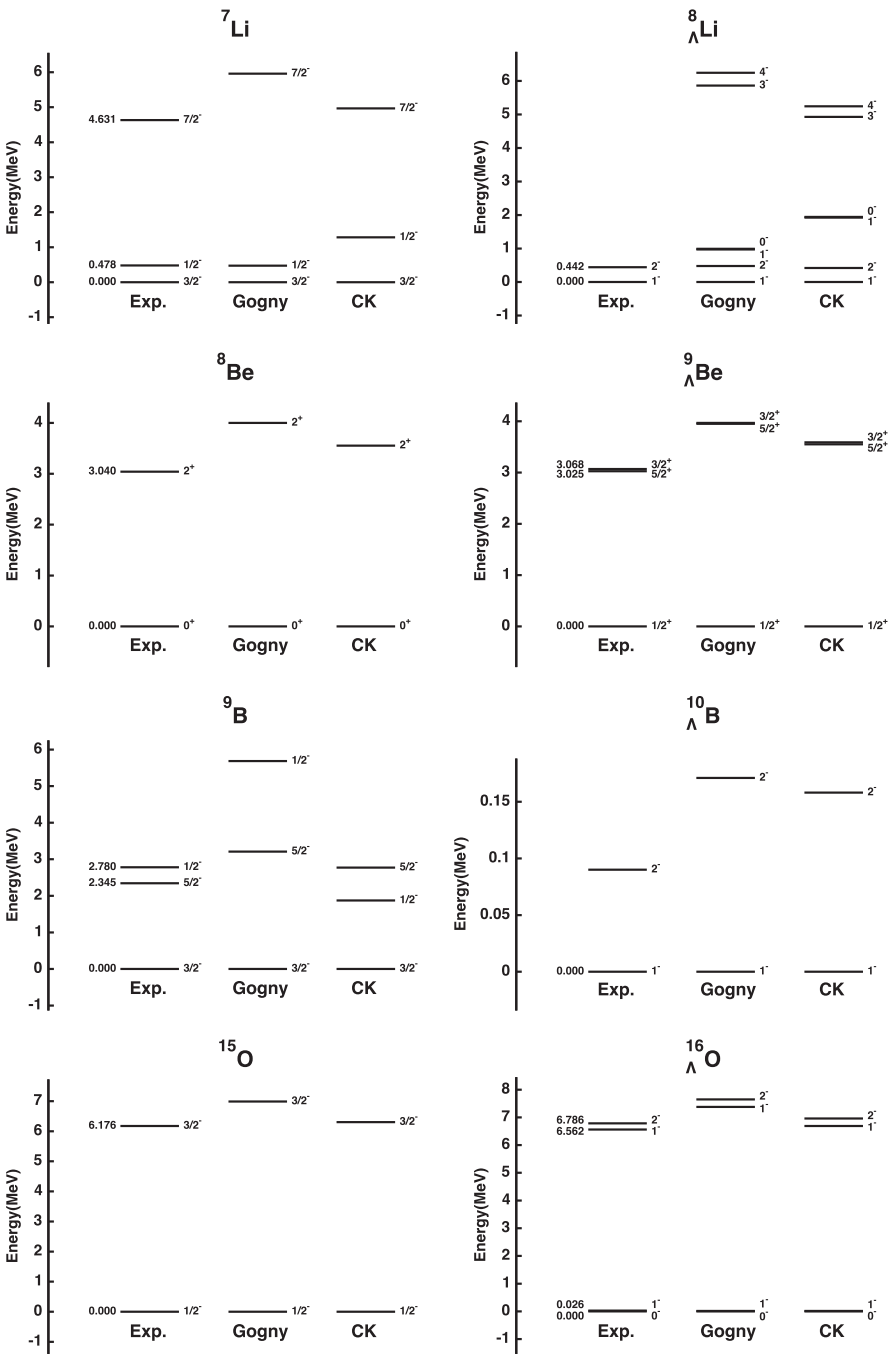

Figure 2. Spectra for *p*-shell hypernuclei $^{8}_{\Lambda}$Li, $^{9}_{\Lambda}$Be, $^{10}_{\Lambda}$B and $^{16}_{\Lambda}$O, and adjacent nuclei, calculated by the Gogny+ΛN interaction (indicated by Gogny) and by the (8-16) TBME(CK)+ΛN interaction [41] (indicated by CK), compared with experimental data [33]. The experimental spectra of adjacent nuclei are taken from [53].

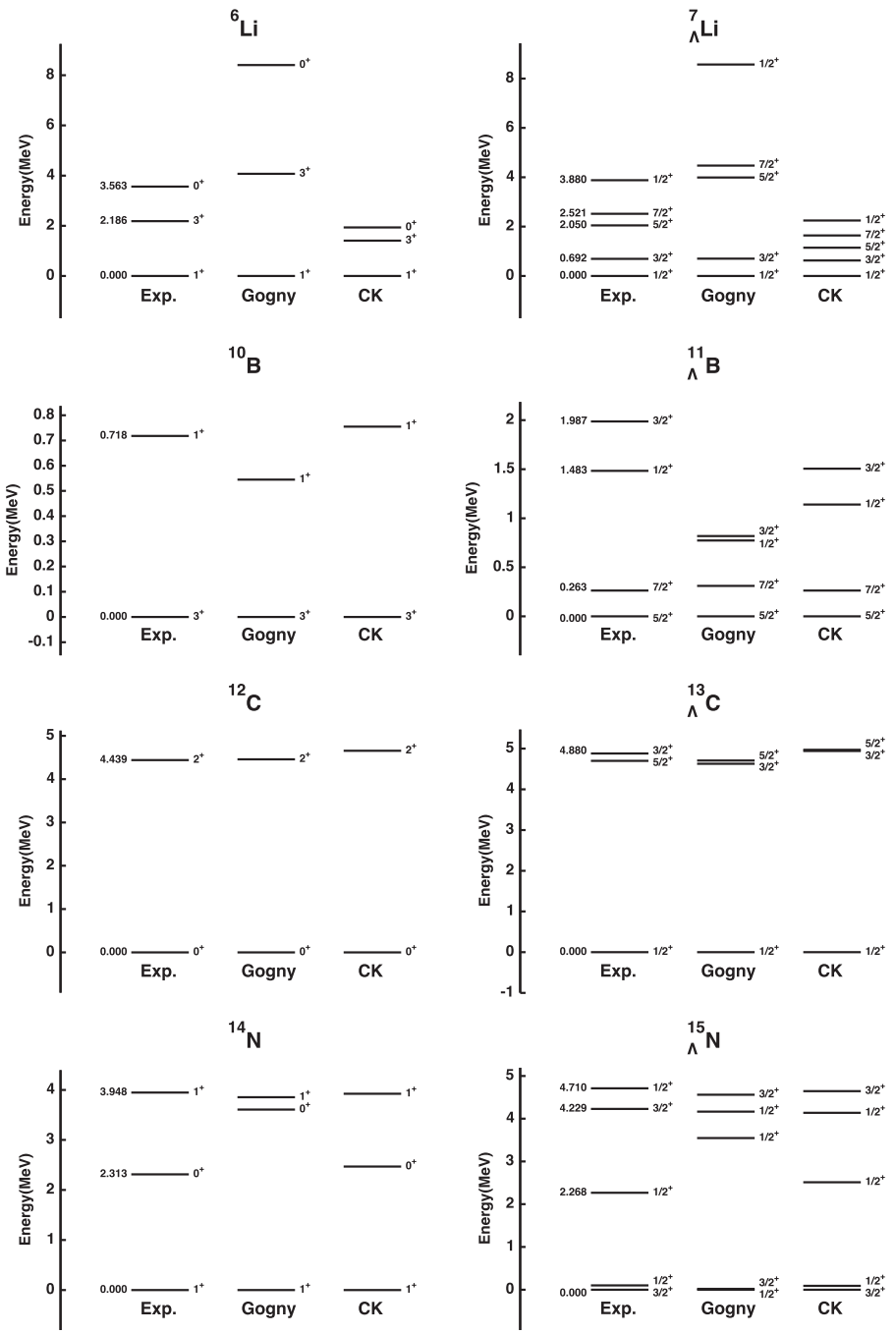

Figure 3. Similar to figure 2, but for ${}^{7}_{\Lambda}$Li, ${}^{11}_{\Lambda}$B, ${}^{13}_{\Lambda}$C, and ${}^{15}_{\Lambda}$N and their adjacent nuclei. The experimental levels without energy numbering means that their energies have not been resolved exactly in experiments. The data are from [53] for nuclei and [33] for hypernuclei.

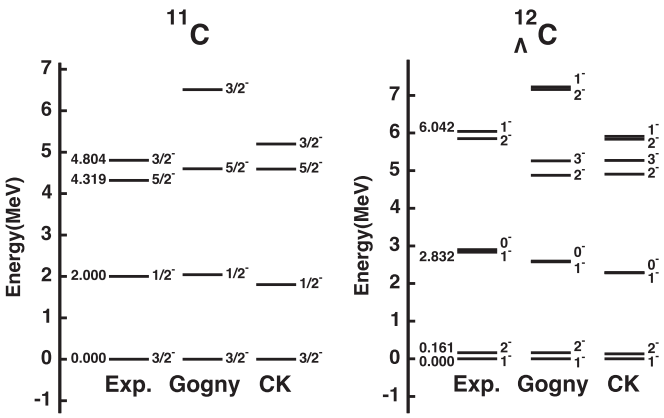

Figure 4. Similar to figures 2 and 3, but for ^{11}C and $^{12}_{\Lambda}$C. The experimental data are from [53] for ^{11}C and [54] for $^{12}_{\Lambda}$C.

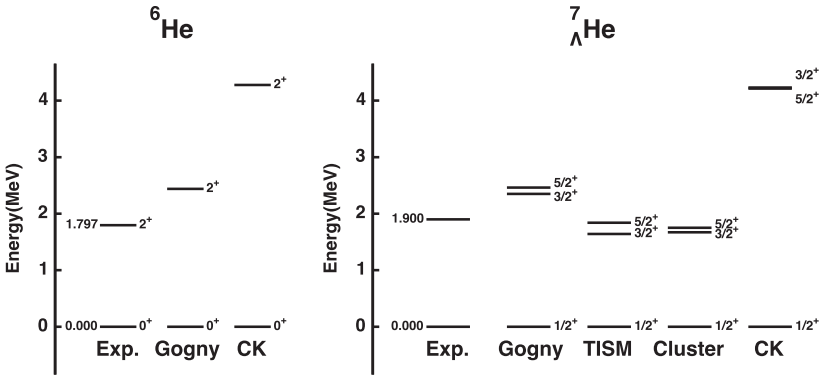

Figure 5. Similar to figures 2 and 3, but for ^{6}He and $^{7}_{\Lambda}$He, compared with the calculations by translational invariant shell-model (TISM) [57], four-body cluster model (Cluster) [58]. The experimental data are from [53] for ^{6}He and [56] for $^{7}_{\Lambda}$He.

The electroproduction of the hypernucleus $^{9}_{\Lambda}$Li was studied on a ^{9}Be target with sub-MeV energy resolution [59]. Four levels were obtained by fitting the ^{9}Be$(e, e'\mathrm{K}^{+})^{9}_{\Lambda}$Li spectrum. Figure 6 shows the experimental level energies [59] and calculations by the shell-model with the Gongny+ΛN, CK+ΛN, and Millener's calculation [8] which used the ^{8}Li spectrum and ΛN interaction. The experiment [59] has not pinned down the spins and parities of the states, but the first two levels were assumed to be the $5/2^{+}-3/2^{+}$ doublet. The third experimental peak observed in the ^{9}Be$(e, e'\mathrm{K}^{+})^{9}_{\Lambda}$Li spectrum was assigned as a mixture of $3/2^{+}$ and $1/2^{+}$ states with a doublet spacing <0.1 MeV which cannot be resolved with the energy resolution of 730 keV in the experiment [59]. The fourth experimental peak was assumed to be the second $5/2^{+}$ state [59]. Our calculation well reproduces the experiment data.

The high-resolution spectroscopy of the hypernucleus $^{10}_{\Lambda}$Be was carried out at JLab, using the ^{10}B$(e, e'\mathrm{K}^{+})^{10}_{\Lambda}$Be reaction, with a resolution of $\sim$0.78 MeV [60]. Four levels were obtained. Figure 7 shows the excitation energies of the levels corresponding to the four

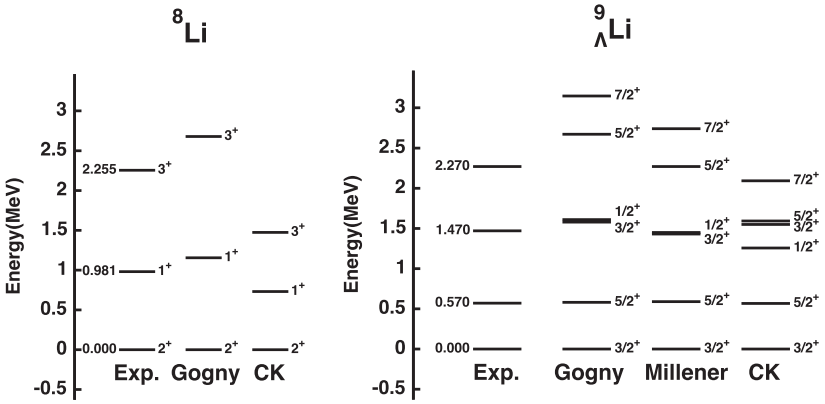

Figure 6. Similar to figures 2–4, but for ^{8}Li and $^{9}_{\Lambda}$Li. The experimental data are from [53] for ^{8}Li and [59] for $^{9}_{\Lambda}$Li. 'Millener' indicates the calculation by Millener assuming the Λ hyperon coupled to the experimental states of ^{8}Li [8].

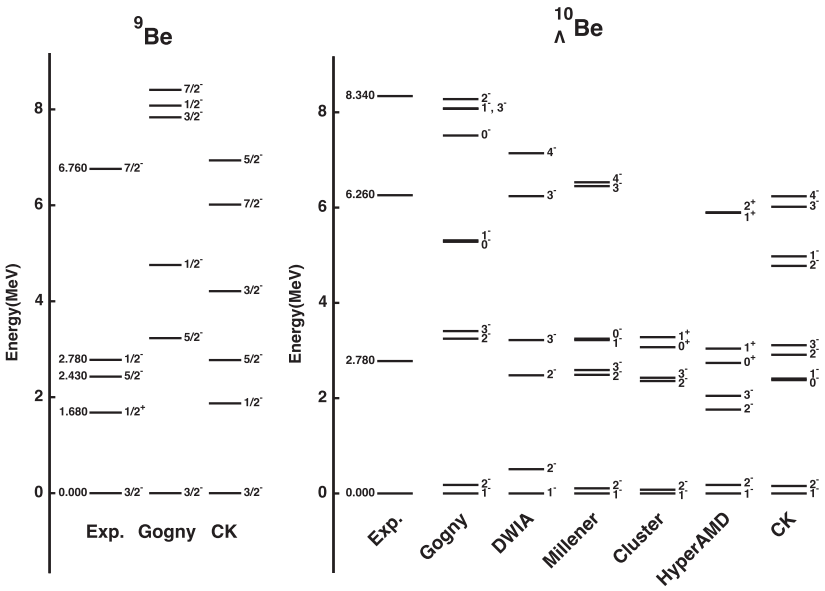

Figure 7. Similar to figures 2–6, but for ^{9}Be and $^{10}_{\Lambda}$Be. Other calculations excepting the Gogny and CK are DWIA [61], Millener [8], four-body cluster model (indicated by Cluster) [62], HyperAMD [63]. The data are from [53] for ^{9}Be and [60] for $^{10}_{\Lambda}$Be.

experimental peaks [60], compared with various calculations. It is rather convincing to assign the first peak to be the mixture of $1^-$and 2^-states. However, various theoretical calculations disagree with each other in the assignment of the second and third levels. The present calculations reproduce well the experimental spectrum, though higher resolution of spectroscopy is needed to confirm the results.

The spectroscopic experiment for the hypernucleus $^{12}_{\Lambda}$B was carried out at JLab, using the ^{11}C(e, e'K$^+$)$^{12}_{\Lambda}$B reaction [64]. Eight peaks in the reaction spectrum were obtained with

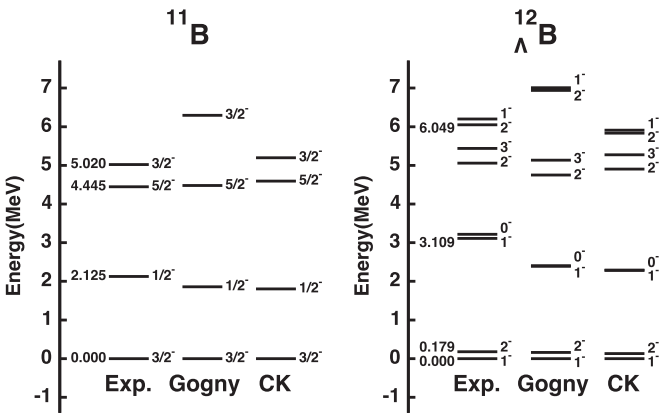

Figure 8. Similar to figures 2–7, but for ^{11}B and $^{12}_{\Lambda}$B. The data are from [53] for ^{11}B and [64] for $^{12}_{\Lambda}$B.

statistical significance larger than 4σ. The first four peaks are considered to have a *s*-shell Λ coupled to ^{11}B that has a negative-parity structure, while other four peaks correspond to Λ in the *p*-shell. In this paper, we can only calculate the states with the Λ in the *s* shell, because we have no ΛN interaction for the *p*-shell Λ. The calculations are given in figure 8. For the negative-parity states in which the Λ stays in the *s* shell, the first two levels are the ground-state doublet states 1_1^- and 2_1^- with a Λ_s coupled to the $3/2^-$ ^{11}B ground state. The third experimental peak is considered to be the lower member of the second doublet (1_2^- and 0_1^-) with ^{11}B in the $1/2^-$configuration. The 0_1^- and 1_3^-, as well as the third doublet (2_2^- and 3_1^-), were predicted to have small cross sections and thus are difficult to be observed without sufficient statistics and a better signal/background ratio [64]. Shell-model calculations based on the Gogny or CK interaction reproduce well the experimental spectra of both ^{11}B and $^{12}_{\Lambda}$B.

The advantage to use the Gogny force is that we can calculate the spectra of a wide range of nuclei without need to adjust parameters. The density-dependent term provides an equivalent three-body force. In general, the Gogny interaction gives better calculations for the neutron-rich *p*-shell hypernuclei than the CK interaction. We have estimated the discrepancy between experimental data and calculations, using $\Delta = \left[\frac{1}{N}\sum(E_{\rm exp} - E_{\rm cal})^2 / E_{\rm exp}^2\right]^{1/2}$, with $E_{\rm exp}$ and $E_{\rm cal}$ being the experimental and calculated energies of an excited level, respectively, and N being the total number of the excited levels considered in figures 2–8. The Gogny interaction gives the overall discrepancies of $\Delta = 0.67$ for all the nuclei investigated, $\Delta = 0.37$ for all the hypernuclei and $\Delta = 0.51$ for the nuclei and hypernuclei together, while the CK interaction gives $\Delta = 0.76$ for the nuclei, $\Delta = 0.38$ for the hypernuclei and $\Delta = 0.57$ for the nuclei and hypernuclei together. We have also checked how the calculations depend on the choice of the Gogny parameterizations. Figure 9 shows the calculations based on the D1S, D1M and D1N sets of the Gogny parameters for the couple of ^{6}He and $^7_{\Lambda}$He as examples. We see that all the parameterizations give reasonable descriptions of the excitation spectra.

Electromagnetic transition strengths are important physical observables. In the present work, we have calculated the reduced electric quadrupole transition probability $B(E2)$, defined by [51]

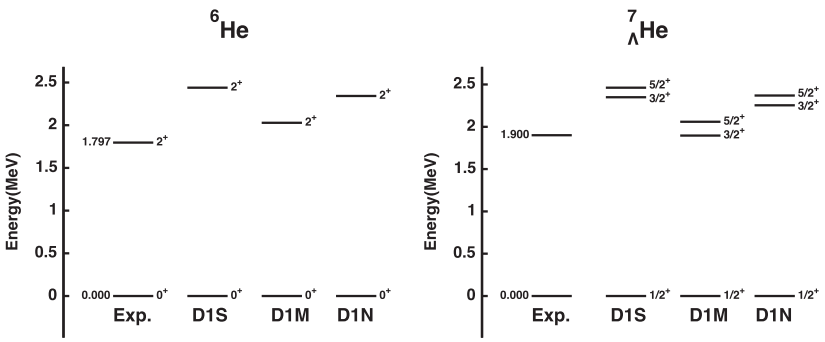

Figure 9. Calculated energy spectra of ^{6}He and $^{7}_{\Lambda}$He with the D1S, D1M, and D1N sets of the Gogny parameters.

Table 1. $B(E2)$ calculations based on the Gogny and CK interactions, compared with experimental data [66, 67] and the cluster-model calculations (indicated by Cluster) given in [65].

	Gogny (e^2fm^4)	CK (e^2fm^4)	Cluster (e^2fm^4)	Exp (e^2fm^4)
$B(E2;\ ^{6}\mathrm{Li}\ 3^+ \to 1^+)$	4.37	4.82	9.62	10.7
$B(E2;\ ^{7}_{\Lambda}\mathrm{Li}\ 5/2^+ \to 1/2^+)$	3.77	4.23	2.42	3.6
$B(E2;\ ^{7}_{\Lambda}\mathrm{Li}\ 5/2^+ \to 3/2^+)$	0.78	0.87	0.74	—
$B(E2;\ ^{7}_{\Lambda}\mathrm{Li}\ 7/2^+ \to 3/2^+)$	4.60	5.09	3.69	—
$B(E2;\ ^{7}_{\Lambda}\mathrm{He}\ 3/2^+ \to 1/2^+)$	0.83	1.16	0.06	—
$B(E2;\ ^{7}_{\Lambda}\mathrm{He}\ 5/2^+ \to 1/2^+)$	0.85	1.16	0.07	—
$B(E2;\ ^{8}\mathrm{Be}\ 2^+ \to 0^+)$	13.63	14.29	—	—
$B(E2;\ ^{9}_{\Lambda}\mathrm{Be}\ 3/2^+ \to 1/2^+)$	13.62	14.89	—	5.7

$$B(E2\colon i \to f) = \frac{|\langle f||O(E2)||i\rangle|^2}{2J_i + 1}, \tag{8}$$

where the $E2$ transition operator is given by $O(E2) = r^2 Y^2_\mu(\hat{r}) e_{tz}$ with the spherical harmonic function Y^2_μ. The effective charge e_{tz} for p-shell nuclei takes the commonly used values of $e_p = 1.5e$ and $e_n = 0.5e$. The single-particle matrix elements for $E2$ operator is given by

$$\langle n_a l_a j_a||O(E2)||n_b l_b j_b\rangle = (-1)^{j_a+1/2}\frac{1 + (-1)^{l_a+2+l_b}}{2} \times \sqrt{\frac{5(2j_a + 1)(2j_b + 1)}{4\pi}} \begin{pmatrix} j_a & 2 & j_b \\ 1/2 & 0 & -1/2 \end{pmatrix} \langle R_{n_a l_a}|r^2|R_{n_b l_b}\rangle e_{tz}, \tag{9}$$

where R_{nl} is the radial components of the HO wave function. The notation is standard with a and b indicating the initial and final states [51]. Table 1 shows the $B(E2)$ calculations based on the Gogny and CK interactions, compared with experimental data and the cluster-model calculations given in [65].

In [66], the authors claimed an experimental evidence that the addition of a Λ hyperon to ^{6}Li nucleus causes the shrinkage of the nuclear size. We use the approximation given in our previous paper [68] to calculate nuclear charge radius, but the Gogny or CK shell-model wavefunctions are used in the calculations. Both Gogny and CK calculations give

$\langle r_{\rm ch}^2\rangle^{1/2} = 2.137$ fm and 2.127 fm for ^{6}Li and $^7_\Lambda$Li, respectively, which leads to a shrinkage of 0.01 fm in the charge radius. The experimental charge radius of ^{6}Li is 2.589 fm [69]. The cluster-model calculations gave the size shrinkage of 0.15–0.33 fm depending on the model parameters used [70]. In the present shell-model calculations, we assume a core, i.e. ^{4}He. The size calculation might need to consider the possible change of the core when a hyperon is added to the nucleus. The model space and $\hbar\omega$ choice would also affect the calculation of nuclear size.

4. Conclusion

We have systematically investigated the excitation spectra of p-shell hypernuclei using shell model with the Gogny+ΛN interaction including the ΛN–ΣN and ΣN–ΣN couplings. With its density-dependence property, the Gogny force can give reasonable descriptions in spectra, binding energies and the electric quadrupole transition probabilities $B(E2)$ for a wide range of p-shell nuclei without adjusting parameters. For $^8_\Lambda$Li, $^9_\Lambda$Be, $^{10}_\Lambda$B, and $^{16}_\Lambda$O, the shell-model calculations with the Gogny+ΛN interaction gives good agreements with γ-ray data. For $^7_\Lambda$Li, $^{11}_\Lambda$B, $^{12}_\Lambda$C, $^{13}_\Lambda$C, and $^{15}_\Lambda$N, some of calculated energy spacings deviate slightly from γ-ray data, but could be improved by further calculations, e.g. by increasing model space and/or adjusting the Gogny parameters specially for shell-model calculations. With the recent high-resolution spectroscopic experiments for $^7_\Lambda$He, $^9_\Lambda$Li, $^{10}_\Lambda$Be, and $^{12}_\Lambda$B performed at JLab, we have compared our calculations with the data as well as other theoretical predictions. Overall agreements have been obtained. We have shown that the Gogny+ΛN interaction provides reasonable descriptions for both nuclei and hypernuclei of the p shell.

Acknowledgments

We would like to thank B Dai and JG Li for their useful comments and discussions. We are also grateful to H Zeng for his help in computing coding. This work has been supported by the National Key R&D Program of China under Grant No. 2018YFA0404401; the National Natural Science Foundation of China under Grants No. 11835001, No. 11575007, No. 11921006 and No. 11847203; the China Postdoctoral Science Foundation under Grant No. 2018M630018, and Beijing innovation research program for undergraduates. We acknowledge the High-Performance Computing Platform of Peking University for providing computational resources.

ORCID iDs

F R Xu https://orcid.org/0000-0001-6699-0965

References

[1] Danysz M and Pniewski J 1953 Delayed disintegration of a heavy nuclear fragment: I *London, Edinburgh, Dublin Phil. Mag. J. Sci.* **44** 348–50
[2] Gal A and Dover C B 1995 Strange hadronic matter *Nucl. Phys.* A **585** 1–12
[3] Schaffner-Bielich J and Gal A 2000 Properties of strange hadronic matter in bulk and in finite systems *Phys. Rev.* C **62** 034311
[4] Schaffner-Bielich J 2008 Hypernuclear physics for neutron stars *Nucl. Phys.* A **804** 309–21
[5] Schaffner-Bielich J 2010 Strangeness in compact stars *Nucl. Phys.* A **835** 279–86

[6] Gal A, Soper J M and Dalitz R H 1971 A shell-model analysis of Λ binding energies for the p-shell hypernuclei. I. Basic formulas and matrix elements for ΛN and ΛNN forces *Ann. Phys., NY* **63** 53–126

[7] Millener D J 2010 Shell-model structure of light hypernuclei *Nucl. Phys.* A **835** 11–8

[8] Millener D J 2012 Shell-model calculations for p-shell hypernuclei *Nucl. Phys.* A **881** 298–309

[9] Reinhard P G 1989 The relativistic mean-field description of nuclei and nuclear dynamics *Rep. Prog. Phys.* **52** 439–514

[10] Sugahara Y and Toki H 1994 Relativistic mean field theory for lambda hypernuclei and neutron stars *Prog. Theor. Phys.* **92** 803–13

[11] Shen H, Yang F and Toki H 2006 Double- hypernuclei in the relativistic mean-field theory *Prog. Theor. Phys.* **115** 325–35

[12] Zhou X R, Schulze H-J, Sagawa H, Wu C X and Zhao E G 2007 Hypernuclei in the deformed Skyrme-Hartree–Fock approach *Phys. Rev.* C **76** 034312

[13] Lu B N *et al* 2011 Quadrupole deformation (β, γ) of light λ hypernuclei in a constrained relativistic mean field model: Shape evolution and shape polarization effect of the λ hyperon *Phys. Rev.* C **84** 014328

[14] Lu B N, Hiyama E, Sagawa H and Zhou S G 2014 Superdeformed λ hypernuclei within relativistic mean field models *Phys. Rev.* C **89** 044307

[15] Cui J-W *et al* 2017 Investigation of single-and double-λ hypernuclei using a beyond-mean-field approach *Phys. Rev.* C **95** 024323

[16] Wu X Y, Mei H, Yao J M and Zhou X R 2017 Beyond-mean-field study of the hyperon impurity effect in hypernuclei with shape coexistence *Phys. Rev.* C **95** 034309

[17] Li W Y, Cui J W and Zhou X R 2018 Structure of ${}^{9}_{\Lambda}Be$ and ${}^{10}_{\Lambda\Lambda}Be$ using the beyond-mean-field Skyrme-Hartree-Fock approach *Phys. Rev.* C **97** 034302

[18] Dalitz R H, Herndon R C and Tang Y C 1972 Phenomenological study of s-shell hypernuclei with ΛN and ΛNN potentials *Nucl. Phys.* B **47** 109–37

[19] Gal A, Soper J M and Dalitz R H 1978 A shell-model analysis of Λ binding energies for the p-shell hypernuclei III. Further analysis and predictions *Ann. Phys., NY* **113** 79–97

[20] Dalitz R H and Gal A 1978 The formation of, and the γ-radiation from, the p-shell hypernuclei *Ann. Phys., NY* **116** 167–243

[21] Millener D J, Gal A, Dover C B and Dalitz R H 1985 Spin dependence of the ΛN effective interaction *Phys. Rev.* C **31** 499

[22] Auerbach E H, Baltz A J, Dover C B, Gal A, Kahana S H, Ludeking L and Millener D J 1983 Hypernuclear spectroscopy in the p shell *Ann. Phys., NY* **148** 381–435

[23] Itonaga K, Motoba T and Bandō H 1990 p-shell hypernuclei via (K^-, π^-), (π^+, K^+) and (stopped K^-, π^-) reactions: a systematic calculation with configuration mixing *Prog. Theor. Phys.* **84** 291–316 08

[24] Millener D J 2001 Shell-model description of Λ hypernuclei *Nucl. Phys.* A **691** 93–100

[25] Motoba T, Bando H and Ikeda K 1983 Light p-shell -hypernuclei by the microscopic three-cluster model *Prog. Theor. Phys.* **70** 189–221

[26] Motoba T, Bando H, Ikeda K and Yamada T 1985 Chapter III. Production, structure and decay of light p -shell Λ-hypernuclei *Prog. Theor. Phys. Suppl.* **81** 42–103

[27] Yamamoto Y and Bando H 1990 Hypernuclear properties derived from the Nijmegen Soft-Core OBE potential *Prog. Theor. Phys.* **83** 254–64

[28] Akaishi Y, Harada T, Shinmura S and Myint K S 2000 Coherent Λ–Σ coupling in s-shell hypernuclei *Phys. Rev. Lett.* **84** 3539–41

[29] Myint K S, Harada T, Shinmura S and Akaishi Y 2000 *Few-Body Probl. Phys. '99* ed S Oryu, M Kamimura and S Ishikawa (Vienna: Springer) pp 383–6

[30] Maessen P M M, Rijken T A and de Swart J J 1989 Soft-core baryon-baryon one-boson-exchange models: II. Hyperon–nucleon potential *Phys. Rev.* C **40** 2226–45

[31] Rijken T A, Stoks V G J and Yamamoto Y 1999 Soft-core hyperon-nucleon potentials *Phys. Rev.* C **59** 21–40

[32] Rijken T A and Yamamoto Y 2006 Extended-soft-core baryon-baryon model: II. Hyperon–nucleon interaction *Phys. Rev.* C **73** 044008

[33] Tamura H *et al* 2013 Gamma-ray spectroscopy of hypernuclei present and future *Nucl. Phys.* A **914** 99–108

[34] Umeya A and Harada T 2011 Doublet-spacing enhancement caused by $\Lambda N - \Sigma N$ coupling in ${}_{\Lambda}$Li hypernuclear isotopes *Phys. Rev.* C **83** 034310

[35] Umeya A and Harada T 2009 Λ–Σ coupling effect in the neutron-rich Λ hypernucleus $^{10}_{\Lambda}$Li in a microscopic shell-model calculation *Phys. Rev.* C **79** 024315

[36] Gal A and Millener D J 2013 Neutron-rich hypernuclei: $^{6}_{\Lambda}H$ and beyond *Phys. Lett.* B **725** 450

[37] Gal A and Millener D J 2011 Shell-model predictions for ΛΛ hypernuclei *Phys. Lett.* B **701** 342–5

[38] Millener D J 2008 Shell-model interpretation of γ-ray transitions in p-shell hypernuclei *Nucl. Phys.* A **804** 84–98

[39] Gal A 2015 Charge symmetry breaking in Λ hypernuclei revisited *Phys. Lett.* B **744** 352–7

[40] Wirth R, Gazda D, Navrátil P and Roth R 2018 Hypernuclear no-core–shell model *Phys. Rev.* C **97** 064315

[41] Cohen S and Kurath D 1965 Effective interactions for the 1p shell *Nucl. Phys.* **73** 1–24

[42] Green I M and Moszkowski S A 1965 Nuclear coupling schemes with a surface delta interaction *Phys. Rev.* **139** B790–3

[43] Sagawa H, Brown B A and Scholten O 1985 Shell-model calculations with a Skyrme-type effective interaction *Phys. Lett.* B **159** 228–32

[44] Dechargé J and Gogny D 1980 Hartree–Fock–Bogolyubov calculations with the D 1 effective interaction on spherical nuclei *Phys. Rev.* C **21** 1568–93

[45] Goriely S, Hilaire S, Girod M and Péru S 2009 First Gogny–Hartree–Fock–Bogoliubov nuclear mass model *Phys. Rev. Lett.* **102** 242501

[46] Chappert F, Girod M and Hilaire S 2008 Towards a new Gogny force parameterization: impact of the neutron matter equation of state *Phys. Lett.* B **668** 420–4

[47] Jiang W G, Hu B S, Sun Z H and Xu F R 2018 Gogny-force-derived effective shell-model Hamiltonian *Phys. Rev.* C **98** 044320

[48] Gal A, Hungerford E V and Millener D J 2016 Strangeness in nuclear physics *Rev. Mod. Phys.* **88** 035004

[49] Alex Brown B and Richter W A 2006 New 'USD' Hamiltonians for the *sd* shell *Phys. Rev.* C **74** 034315

[50] Jiang W G 2017 Shell-model effective Hamiltonian based on Gogny force *PhD Thesis* Peking University, 7

[51] Alex Brown B 2005 Lecture Notes in Nuclear Structure Physics National Super Conducting Cyclotron Laboratory) https://people.nscl.msu.edu/~brown/Jina-workshop/BAB-lecture-notes.pdf

[52] Qi C and Xu F R 2008 Isospin asymmetry effects in mirror nuclei with modern charge-dependent NN potential *Nucl. Phys.* A **814** 48–65

[53] Burrows T W and Dunford C L 2005 Nuclear information services at the national nuclear data center *AIP Conf. Proc.* vol 769 (New York: AIP) pp 582–5 https://www.nndc.bnl.gov/

[54] Hosomi K *et al* 2015 Precise determination of $^{12}_{\Lambda}C$ level structure by γ-ray spectroscopy *Prog. Theor. Exp. Phys.* **2015** 081D01

[55] Hosomi K *et al* 2013 Gamma-ray spectroscopy of 12λc via the (π+, k+) reaction *Nucl. Phys.* A **914** 184–8

[56] Gogami T *et al* 2016 Spectroscopy of the neutron-rich hypernucleus $^{7}_{\Lambda}$He from electron scattering *Phys. Rev.* C **94** 021302

[57] Richter O, Sotona M and Žofka J 1991 Realistic $A = 7$ hypernuclear productions *Phys. Rev.* C **43** 2753–64

[58] Hiyama E, Isaka M, Kamimura M, Myo T and Motoba T 2015 Resonant states of the neutron-rich Λ hypernucleus $^{7}_{\Lambda}$He *Phys. Rev.* C **91** 054316

[59] Urciuoli G M *et al* 2015 Spectroscopy of $^{9}_{\Lambda}$Li by electroproduction *Phys. Rev.* C **91** 034308

[60] Gogami T *et al* 2016 High resolution spectroscopic study of $^{10}_{\Lambda}$Be *Phys. Rev.* C **93** 034314

[61] Motoba T, Bydžovský P, Sotona M and Itonaga K 2010 Spectroscopy of electro- and photo-productions of hypernuclei *Prog. Theor. Phys. Suppl.* **185** 224–51

[62] Hiyama E and Yamamoto Y 2012 Structure of ^{10}Be and ^{10}B hypernuclei studied with the four-body cluster model *Prog. Theor. Phys.* **128** 105–24

[63] Isaka M, Homma H, Kimura M, Dote A and Ohnishi A 2013 Structure of Be hyper isotopes *Few-Body Syst.* **54** 1219–22

[64] Tang L *et al* 2014 Experiments with the high resolution Kaon spectrometer at JLab Hall C and the new spectroscopy of $^{12}_{\Lambda}$B hypernuclei *Phys. Rev.* C **90** 034320

[65] Hiyama E, Kamimura M, Miyazaki K and Motoba T 1999 γ transitions in $a = 7$ hypernuclei and a possible derivation of hypernuclear size *Phys. Rev.* C **59** 2351

[66] Tanida K *et al* 2001 Measurement of the B(E2) of ${}^{7}_{\Lambda}$Li and shrinkage of the hypernuclear size *Phys. Rev. Lett.* **86** 1982
[67] Akikawa H *et al* 2002 Hypernuclear fine structure in ${}^{9}_{\Lambda}$*Be Phys. Rev. Lett.* **88** 082501
[68] Hu B S *et al* 2016 Ab initio nuclear many-body perturbation calculations in the Hartree–Fock basis *Phys. Rev.* C **94** 014303
[69] Angeli I and Marinova K P 2013 Table of experimental nuclear ground state charge radii: an update *At. Data Nucl. Data Tables* **99** 69–95
[70] Kanada-En'yo Y 2018 Excitation energy shift and size difference of low-energy levels in p-shell λ hypernuclei *Phys. Rev.* C **97** 024330